Evolution of the Fermi Surface of the Electron-Doped High-Temperature Superconductor $Nd_{2-x}Ce_xCuO_4$ Revealed by Shubnikov–de Haas Oscillations

T. Helm,[1] M. V. Kartsovnik,[1] M. Bartkowiak,[2] N. Bittner,[1] M. Lambacher,[1] A. Erb,[1] J. Wosnitza,[2] and R. Gross[1,3]

[1]*Walther-Meißner-Institut, Bayerische Akademie der Wissenschaften, D-85748 Garching, Germany*

[2]*Hochfeld-Magnetlabor Dresden, Forschungszentrum Dresden-Rossendorf, D-01328 Dresden, Germany*

[3]*Physik-Department, Technische Universität München, D-85748 Garching, Germany*

(Received 19 May 2009; published 5 October 2009)

We report on the direct probing of the Fermi surface in the bulk of the electron-doped superconductor $Nd_{2-x}Ce_xCuO_4$ at different doping levels by means of magnetoresistance quantum oscillations. Our data reveal a sharp qualitative change in the Fermi surface topology, due to translational symmetry breaking in the electronic system which occurs at a critical doping level significantly exceeding the optimal doping. This result implies that the $(\pi/a, \pi/a)$ ordering, known to exist at low doping levels, survives up to the overdoped superconducting regime.

DOI: 10.1103/PhysRevLett.103.157002 PACS numbers: 74.25.Jb, 71.18.+y, 74.20.Mn, 74.72.Jt

The Fermi surface topology and its evolution with doping is one of the most important issues related to the nature of charge carriers and various competing ordering phenomena in the high-temperature superconducting cuprates. The research has been pushed forward immensely by the recent discovery of slow magnetic quantum oscillations in the hole-underdoped superconductors $YBa_2Cu_3O_{6.5}$ [1–3] and $YBa_2Cu_4O_8$ [4,5]. While the general trend is to associate these oscillations with small Fermi surface pockets, the latter apparently contradict the discontinuous Fermi arcs scenario derived from angle-resolved photoemission (ARPES) experiments [6] and their origin is currently a matter of hot debate [1,3,5,7–15]. To solve the problem, it is pivotal to understand how the Fermi surface develops with changing the concentration and even the sign of charge carriers. However, direct probing of the Fermi surface by means of magnetic quantum oscillations has been restricted so far to hole-doped compounds with few selected doping levels, namely, to the above mentioned underdoped yttrium-barium cuprates characterized by highly ordered oxygen and to cleanest samples of strongly overdoped $Tl_2Ba_2CuO_{6+\delta}$ [16]. Here we report the observation of quantum oscillations in the interlayer magnetoresistance of the electron-doped superconductor $Nd_{2-x}Ce_xCuO_4$ (NCCO) at the optimal, $x = 0.15$, as well as overdoped, $x = 0.16$ and 0.17, compositions. The data obtained provide direct evidence for a well-defined closed Fermi surface (rather than Fermi arcs) and clearly reveal its evolution with doping level. In particular, a dramatic change in the oscillation spectrum observed at increasing x from 0.16 to 0.17 is indicative of a topological transformation of the Fermi surface in the overdoped regime.

Compared to hole-doped cuprates, the electron-doped NCCO has a few advantages. First, the superconducting state of NCCO is restricted to the narrow doping interval $0.13 \leq n \leq 0.18$ (Fig. 1), where n is the number of doped electrons per Cu ion and $n = x$ due to the well-defined valences of the Nd^{3+} and Ce^{4+} ions. Hence, the whole relevant doping range can be controllably scanned by slightly varying x. Second, the upper critical field of NCCO does nod exceed 10 T [17] which is about an order of magnitude lower than for hole-doped superconductors. Thus, for any doping level, it is easy to suppress superconductivity at low temperatures by applying magnetic field (Fig. 1). This excludes potential ambiguities and complications in the interpretation of magnetic quantum oscillations associated with the vortex state of superconductors [13–15,18]. Finally, the Fermi surface of NCCO is

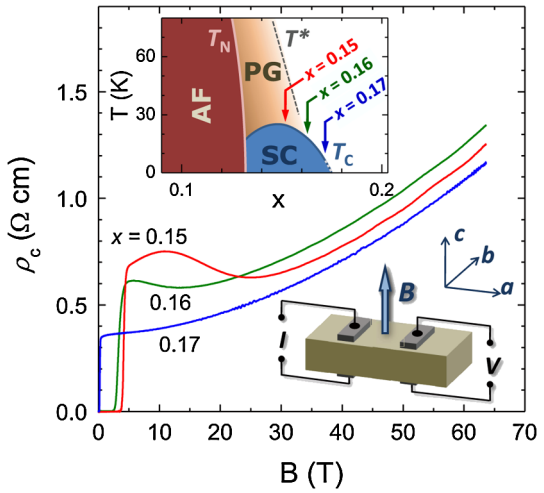

FIG. 1 (color online). c-axis resistivity ρ_c of NCCO plotted vs magnetic field applied perpendicular to the CuO_2 planes at $T = 4$ K for different doping levels x. The upper inset shows schematically the currently accepted phase diagram of NCCO with the superconducting (SC), antiferromagnetic (AF), and pseudogap (PG) regions. The arrows mark the compositions studied in this work. The lower inset illustrates the geometry of the experiment.

expected to be relatively simple: the material only contains a single conducting CuO_2 layer per unit cell, avoiding ambiguities with any bilayer potential [5,9].

Single crystals of NCCO were grown in an Ar/O_2 atmosphere using the travelling solvent floating zone method and annealed in pure argon at 950 °C for 20 h in order to remove interstitial oxygen and strain in the crystal lattice. The high quality of the samples was ensured by structural analysis as well as by magnetic and resistive measurements. The superconducting transition temperatures (taken as the midpoint of the transition in magnetic susceptibility) were $T_c = 23.5$, 19.2, and 5.9 K for the crystals with $x = 0.15$, 0.16, and 0.17, respectively, in agreement with detailed phase diagram studies [19]. The transition widths were <1 K, 2.5 K, and 3.5 K for $x = 0.15$, 0.16, and 0.17, respectively, thus, ensuring homogeneity of Ce doping within ~0.25%. Measurements of the interlayer resistance were performed using an ac current of 0.4–1.0 mA at a frequency of 67 kHz. The magnetic field was applied perpendicular to the CuO_2 planes ($\mathbf{B} \parallel c$-axis), using a 70 T pulse magnet with a pulse duration of 150 ms at the Hochfeld-Magnetlabor Dresden. While the data presented here were taken at the decaying part of the pulse, they were reproduced, although with a higher noise level, at the rising part.

Figure 2(a) shows the oscillatory component of the interlayer resistivity ρ_{osc} of the optimally doped, $x = 0.15$, sample, obtained from the raw data (Fig. 1) after subtracting the monotonic background. The oscillations are periodic in $1/B$ [Fig. 2(b)] with T-independent positions of their maxima and minima, whereas their amplitude A gradually increases upon cooling. Such behavior is a prominent characteristic of the Shubnikov–de Haas (SdH) effect, originating from the Landau quantization of the quasiparticle spectrum [20]. It, thus, provides clear evidence for a well-defined closed Fermi surface, made up of fermionic charge carriers. The oscillation frequency, $F_{0.15} = (290 \pm 10)$ T, yields the area of the extremal Fermi surface cross section, $S_{0.15} = 2\pi e F_{0.15}/\hbar = (2.75 \pm 0.10)$ nm^{-2}. This area amounts to only 1.1% of the two-dimensional Brillouin zone, $S_{\mathrm{BZ}} = (2\pi/a)^2 = 253$ nm^{-2}, where $a = 3.95$ Å is the in-plane lattice constant of NCCO.

The whole data set in Fig. 2(a) can be described by the standard Lifshitz-Kosevich (LK) formula for magnetic quantum oscillations [20]:

$$\rho_{\mathrm{osc}} \propto B^{1/2} R_T R_D \sin(2\pi F/B + \gamma), \qquad (1)$$

where $R_T = \alpha T/B \sinh(\alpha m_c T/B)$ and $R_D = \exp(-\alpha m_c T_D/B)$ are, respectively, the temperature and scattering damping factors, $\alpha = 14.69$ T/K, m_c is the effective cyclotron mass in units of the free electron mass, T_D is the Dingle temperature determined by scattering, and γ is the temperature and field independent Onsager phase. Figures 2(c) and 2(d) show examples of

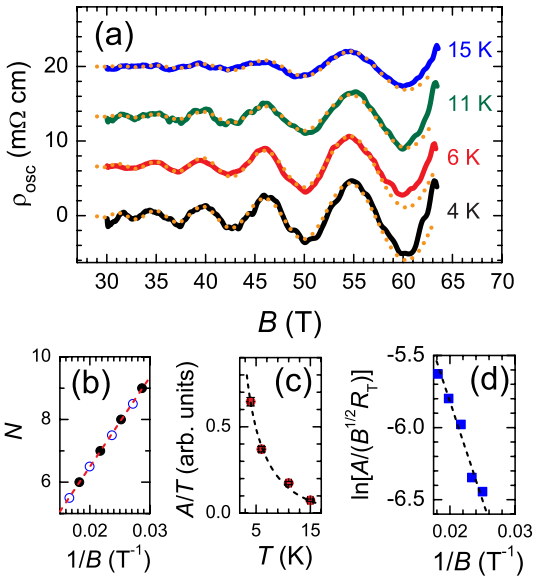

FIG. 2 (color online). (a) Oscillatory part of the interlayer resistivity of optimally doped NCCO as a function of a magnetic field ($\mathbf{B} \parallel c$ axis) at different T. The dotted lines are LK fits to the data using the values F, m_c, and T_D obtained from plots in (b), (c), and (d), respectively. (b) Positions of the local maxima (solid circles) and minima (open circles) of ρ_{osc} on an inverse field scale. A linear fit (dotted line) yields $F = 290$ T. (c) Temperature dependence of the oscillation amplitude at $B = 55$ T. The dashed line is the LK temperature dependence with $m_c = 0.6 m_e$. (d) Dingle plot of the oscillation amplitude at $T = 4.0$ K, yielding the Dingle temperature $T_D = 15$ K.

the temperature and field dependence of the oscillation amplitude yielding, respectively, the cyclotron mass $m_c = 0.6 \pm 0.05$ and Dingle temperature $T_D \approx 15$ K. The latter provides an estimate for the scattering time $\tau \simeq \hbar/2\pi k_B T_D \approx 0.8 \times 10^{-13}$ s. This corresponds to a mean free path, averaged over the cyclotron orbit, of $\ell \sim \hbar(S/\pi)^{1/2}\tau/m_c \approx 14$ nm. Using the above mentioned values for F, m_c, and T_D, we obtain a remarkably good fit of the experimental data to Eq. (1) in the entire temperature and field range studied, as demonstrated by dotted lines in Fig. 2(a).

The moderately overdoped sample ($x = 0.16$) shows similar quantum oscillations, however, with only about half the amplitude [Fig. 3(a)]. The oscillation frequency, $F_{0.16} = (280 \pm 15)$ T, is almost the same as for optimal doping. Whereas the overall behavior is similar for the $x = 0.15$ and $x = 0.16$ samples, a drastic change is observed on further increasing the doping level to $x = 0.17$. The slow SdH oscillations vanish and, instead, fast oscillations, also periodic in $1/B$, emerge at fields above 60 T [Fig. 3(b)]. Their frequency, $F_{0.17} = (10.7 \pm 0.4) \times 10^3$ T, corresponds to a large cyclotron orbit on the Fermi surface enclosing the area $S_{0.17} = (102 \pm 4)$ nm^{-2} in $\mathbf{k}$ space or, equivalently, $(0.405 \pm 0.015) S_{\mathrm{BZ}}$.

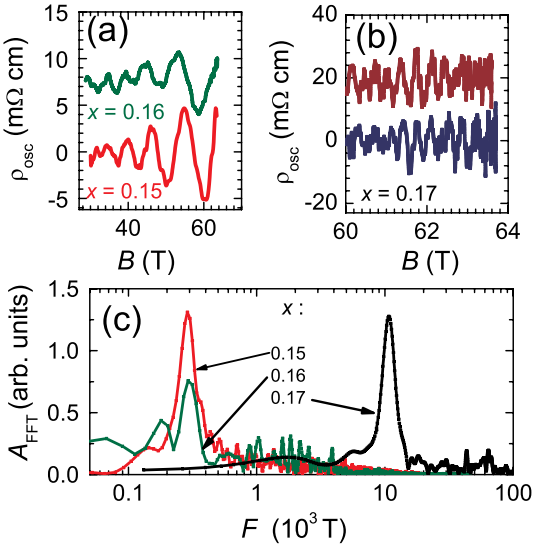

FIG. 3 (color online). Doping dependence of SdH oscillations in NCCO. (a) Slow oscillations in the optimally doped and slightly overdoped ($x = 0.16$) samples at $T = 4.0$ K. (b) Fast oscillations in the sample with $x = 0.17$; $T = 3.5$ K. Data from two different field pulses are shown. (c) Corresponding fast Fourier transform spectra of the oscillatory resistivity. For $x = 0.17$, the spectrum corresponds to an average of the two data sets shown in (b).

The markedly different F obtained for the strongly overdoped ($x = 0.17$) sample on the one hand and for the optimally doped ($x = 0.15$) and slightly overdoped ($x = 0.16$) samples on the other hand becomes apparent in Fig. 3(c). For $x = 0.17$, the interpretation of our data is straightforward: the size of the cyclotron orbit is fully consistent with the results of band-structure calculations [21] and ARPES [22,23] suggesting a single Fermi cylinder centered at the corner of the Brillouin zone, as shown in Fig. 4(a). For $x = 0.17$, we expect $S_{0.17} = 0.415 S_{BZ}$ in perfect agreement with our experimental result. In contrast, the slow oscillations observed at the lower doping levels reveal a very small Fermi surface, indicating a qualitative change in its topology. This suggests that we do not deal with a conventional gradual evolution of the Fermi surface with doping, but rather with a reconstruction due to a broken symmetry. This transformation can be explained by assuming that the commensurate density-wave superstructure, appearing in the electronic system of undoped and underdoped NCCO [23], survives in the optimally doped and even slightly overdoped regime [24]. The ordering potential splits the original conduction band described by the dispersion [25,26]:

$$\varepsilon_{\mathbf{k}} = -2t(\cos ak_x + \cos ak_y) + 4t' \cos ak_x \cos ak_y - 2t''(\cos 2ak_x + \cos 2ak_y) + \mu, \quad (2)$$

where μ is the chemical potential determined by the doping level, into two bands

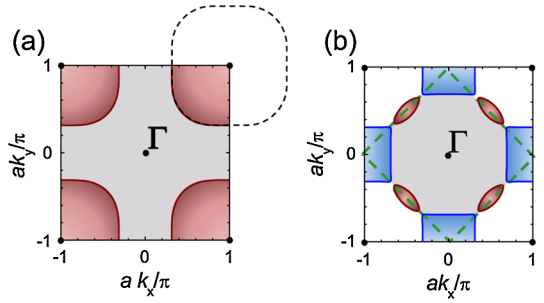

FIG. 4 (color online). (a) Single-component Fermi surface with a cross-sectional area equal to $\approx 41\%$ of the first Brillouin zone corresponding to $x = 0.17$. The dashed line shows the large closed orbit, in the extended zone representation, responsible for the SdH oscillations. (b) Reconstructed Fermi surface comprising one electron and two hole pockets in the reduced Brillouin zone (dashed line). The hole pockets are responsible for the slow oscillations observed on the $x = 0.15$ and 0.16 crystals.

$$\varepsilon_{\mathbf{k}}^{\pm} = \frac{\varepsilon_{\mathbf{k}} + \varepsilon_{\mathbf{k}+\mathbf{Q}}}{2} \pm \sqrt{\left(\frac{\varepsilon_{\mathbf{k}} - \varepsilon_{\mathbf{k}+\mathbf{Q}}}{2}\right)^2 + \Delta^2}. \quad (3)$$

Here, $\mathbf{Q} = (\pi/a, \pi/a)$ is the superstructure wave vector and Δ is the energy gap between the lower and upper bands determined by the strength of the superstructure potential. As a result, the original large Fermi surface is folded and split, forming one electron and two small hole pockets in the new Brillouin zone as shown in Fig. 4(b). Assuming that the slow SdH oscillations originate from the hole pockets and using literature values for the effective overlap integrals [25,26]: $t = 0.38$ eV, $t' = 0.32t$, and $t'' = 0.5t'$, one can apply Eqs. (2) and (3) to fit the size of the pockets to that obtained from the oscillation frequency, with the gap Δ as the fitting parameter. This yields $\Delta = 64$ meV ($x = 0.15$) and 36 meV ($x = 0.16$). Alternatively, one could ascribe the oscillations to the remaining electron pocket by assuming a much larger gap which would completely destroy the hole pockets. However, this would imply an unreasonably large gap, $\Delta = 0.64$ eV, comparable to that in the undoped mother compound [23]. Moreover, in this case the carrier concentration $n = 4S_{0.15}/S_{BZ} \approx 0.045$ electrons per copper site would be totally inconsistent with the nominal value, $n = 0.15$, for optimal doping. Hence, it is most likely that the SdH oscillations originate from the small hole pockets of a reconstructed Fermi surface.

It is tempting to assign the observed transition from a Fermi surface made of small pockets at $x \leq 0.16$ to a large Fermi surface at $x = 0.17$ to a topological change at a critical doping level. Although this scenario is likely, at present we cannot unequivocally rule out the Fermi-surface reconstruction at $x = 0.17$ due to a possible magnetic breakdown [20], allowing charge carriers to tunnel through a small gap which separates different parts of the Fermi surface in $\mathbf{k}$-space. In our case, small orbits on the

reconstructed Fermi surface [Fig. 4(b)] would be considerably suppressed, giving way to the large orbit shown in Fig. 4(a) at a field exceeding the breakdown field $B_{\mathrm{MB}} \simeq 4\Delta^2 m_c/\hbar e \varepsilon_F$. Here, ε_F is the Fermi energy taken from the top of the conduction band. While more detailed data is necessary for a quantitative analysis, we already can estimate the upper limit for the superstructure gap at $x = 0.17$ to $\Delta_{0.17} \leq 8$ meV by setting $B_{\mathrm{MB},0.17} \leq 30$ T.

The combined data of our study and recent experiments [1–5] suggests that in both hole- and electron-doped superconducting cuprates the Fermi surface undergoes a reconstruction below a certain doping level. Whereas for the hole-doped cuprates no conclusive data on the evolution of the Fermi surface around optimal doping is available so far, our study of the electron-doped NCCO clearly shows that the reconstructed Fermi surface is present at optimum doping and even persists into the overdoped regime. This conclusion is consistent with the in-plane magnetotransport studies [19,26,27] suggesting the existence of two types of carriers in electron-overdoped superconductors and pointing to the dominant role of holelike carriers in conductivity.

On the other hand, our results apparently contradict ARPES and inelastic neutron scattering data on NCCO. In the ARPES experiments [22,23], no small holelike Fermi pockets were observed. Instead, a finite spectral weight at the intersections of the large Fermi surface with the reduced Brillouin zone boundary [dashed line in Fig. 4(b)] was reported for optimally and overdoped samples, suggesting no long-range ordering. The recent neutron scattering measurements [28] have revealed an antiferromagnetic correlation length $\xi_{\mathrm{AF}} \leq 5$ nm in optimally doped NCCO. However, our observation of the slow SdH oscillations in samples with $x = 0.15$ and 0.16 starting from $B \approx 30$ T implies the correlation length being at least of the order of the size of the coherent cyclotron orbit, $\sim 2p_F/eB \approx 40$ nm, taking the average in-plane Fermi momentum $p_F = \hbar(S_{0.15}/\pi)^{1/2} \approx 10^{-25}\,\mathrm{kg\,m\,s^{-2}}$. A similar problem holds for the hole-underdoped $YBa_2Cu_3O_{6.5}$ and $YBa_2Cu_4O_8$: the quantum oscillations point to a long-range ordering, which has not been revealed by any other experiment so far. While further studies are necessary for establishing the exact origin of the $(\pi/a, \pi/a)$ ordering revealed by the quantum oscillations, a plausible scenario is a field-induced antiferromagnetic ordering [11]. Indeed, indications of enhanced antiferromagnetic correlations in a magnetic field have been reported both for hole-doped [29,30] and for electron-doped [31] cuprate superconductors.

We thank W. Biberacher for valuable discussions, and the staff of Walther-Meißner-Institut, the Hochfeld-Magnetlabor Dresden-Rossendorf, and the Kristalllabor of TUM for technical assistance. The work was supported by EuroMagNET under the EU Contract No. RII3-CT-2004-506239, by the German Science Foundation via the Research Unit FOR 538, and by the German Excellence Initiative via the Nanosystems Initiative Munich.

[1] N. Doiron-Leyraud *et al.*, Nature (London) **447**, 565 (2007).
[2] C. Jaudet *et al.*, Phys. Rev. Lett. **100**, 187005 (2008).
[3] S. E. Sebastian *et al.*, Nature (London) **454**, 200 (2008).
[4] E. A. Yelland *et al.*, Phys. Rev. Lett. **100**, 047003 (2008).
[5] A. F. Bangura *et al.*, Phys. Rev. Lett. **100**, 047004 (2008).
[6] A. Damascelli, Z. Hussain, and Z.-X. Shen, Rev. Mod. Phys. **75**, 473 (2003).
[7] A. J. Millis and M. R. Norman, Phys. Rev. B **76**, 220503 (R) (2007).
[8] D. LeBoeuf *et al.*, Nature (London) **450**, 533 (2007).
[9] D. Podolsky and H.-Y. Kee, Phys. Rev. B **78**, 224516 (2008).
[10] P. A. Lee, Rep. Prog. Phys. **71**, 012501 (2008).
[11] W.-Q. Chen *et al.*, Europhys. Lett. **82**, 17 004 (2008).
[12] R. K. Kaul *et al.*, Nature Phys. **4**, 28 (2008).
[13] I. Dimov *et al.*, Phys. Rev. B **78**, 134529 (2008).
[14] A. S. Alexandrov, J. Phys. Condens. Matter **20**, 192202 (2008).
[15] X. Jia, P. Goswami, and S. Chakravarty, arXiv:0811.1056 [Phys. Rev. B. (to be published)].
[16] B. Vignolle *et al.*, Nature (London) **455**, 952 (2008).
[17] Y. Wang *et al.*, Science **299**, 86 (2003).
[18] T. Maniv *et al.*, Rev. Mod. Phys. **73**, 867 (2001).
[19] M. Lambacher, Ph.D. thesis, Technische Universität München, 2008.
[20] A. A. Abrikosov, *Fundamentals of the Theory of Metals* (Elsevier Science Publishers B. V., Amsterdam, 1988).
[21] S. Massidda *et al.*, Physica (Amsterdam) **157C**, 571 (1989).
[22] H. Matsui *et al.*, Phys. Rev. B **75**, 224514 (2007).
[23] N. P. Armitage *et al.*, Phys. Rev. Lett. **88**, 257001 (2002).
[24] T. Das, R. S. Markiewicz, and A. Bansil, Phys. Rev. Lett. **98**, 197004 (2007); J. Phys. Chem. Solids **69**, 2963 (2008).
[25] O. K. Andersen *et al.*, J. Phys. Chem. Solids **56**, 1573 (1995).
[26] J. Lin and A. J. Millis, Phys. Rev. B **72**, 214506 (2005).
[27] Y. Dagan *et al.*, Phys. Rev. Lett. **92**, 167001 (2004).
[28] E. M. Motoyama *et al.*, Nature (London) **445**, 186 (2007).
[29] B. Lake *et al.*, Nature (London) **415**, 299 (2002).
[30] D. Haug *et al.*, Phys. Rev. Lett. **103**, 017001 (2009).
[31] M. Matsuura *et al.*, Phys. Rev. B **68**, 144503 (2003).